Fair Energy and Data Rate Maximization in UAV-Powered IoT-Satellite Integrated Networks

Giovanni Iacovelli (iD), *Member, IEEE,* Giovanni Grieco (iD), *Graduate Student Member, IEEE,*
Antonio Petrosino (iD), *Graduate Student Member, IEEE,* Luigi Alfredo Grieco (iD), *Senior Member, IEEE,*
and Gennaro Boggia (iD), *Senior Member, IEEE*

Abstract—Non-Terrestrial Networks represent a valuable solution for providing connectivity to Internet of Things (IoT) devices in remote areas, where classical infrastructure is unavailable. Due to the low-power nature of IoT devices, an Unmanned Aerial Vehicle (UAV) can prevent the energy depletion of these Ground Nodes (GNs) by employing Wireless Power Transfer through an array antenna. Starting from the mathematical modeling of such a scenario, two Mixed-Integer Non-Linear Programming problems are formulated to fairly maximize (i) the energy distribution and (ii) the total amount of data transmitted to a Low Earth Orbit CubeSat. Therefore, it is necessary to optimize the drone kinematics, the transmission scheduling plan, and the beamforming vectors of the array antenna. To cope with their non-convexity, both problems are mathematically manipulated to reach a tractable form, for which two optimization algorithms are proposed and their complexity analyzed. To prove the effectiveness of the overall solution, a comprehensive simulation campaign is conducted under several parameter settings, such as number of GNs and UAV antenna elements with different transmission power levels. Finally, the proposal is compared with a baseline, which confirms the superiority of the proposal up to 7 times in terms of total transmitted data.

Index Terms—Unmanned Aerial Vehicle, Internet of Things, Wireless Power Transfer, Satellite, Optimization.

I. INTRODUCTION

The growth of the number of users, as well as the diversity of services, has been enabled primarily by the expansion of traditional terrestrial wireless communication systems [1]. At the same time, emerging applications impose challenging requirements that must be addressed through the technological advancement of innovative telecommunication facilities [2]. In this context, sixth generation (6G) mobile system [3] promises an ubiquitous coverage across Earth that leverages

an integrated access backhaul that unifies space, aerial, and ground infrastructures [4].

In this regard, Space-Air-Ground Integrated Networks (SAGINs) [5] represent a flexible solution to provide wireless access services with high data rate and reliability, which are key enablers for a variety of both civil and military applications, including Earth observation and mapping, intelligent transportation systems, and disaster rescue. Furthermore, recent 3GPP standardization efforts [6]–[9] identified Non-Terrestrial Networks (NTNs) [10], [11] as a solution to grant connectivity where traditional terrestrial infrastructure is not practical or cost-effective. On the one hand, Low Earth Orbit (LEO) satellite constellations are important to provide full-coverage broadband services for ground users through space-ground interconnection. Manufacturing and launching processes for these constellations have matured, enabling the implementation and deployment of these systems at scale [12], [13]. On the other hand, Unmanned Aerial Vehicles (UAVs) [14], also known as drones, have received significant attention due to their flexibility and applicability in manifold scenarios. In particular, network architectures can benefit from their high mobility, easy deployment, and reusability [15]. Specifically, drones play a pivotal role in the realm of the Internet of Things (IoT) [16], representing an enabling technology to provide pervasive connectivity even where the classical communication infrastructure is not available. The IoT allows interconnection between the physical and digital realms, revolutionizing industries by offering disruptive prospects for automation, efficiency, and data-driven decision-making.

Therefore, the integration of satellite and UAV communications in the IoT domain enables real-time monitoring, autonomous operations, and novel solutions across industries such as agriculture, transportation, and surveillance. This combination results in a full ecosystem, propelling progress toward a smarter and more connected society.

Despite the great advantages in terms of seamless and reliable connectivity, the energy lifetime of IoT devices represents a challenging aspect that is usually not taken into account, especially in harsh environments. To this end, Wireless Power Transfer (WPT) [17] has been recognized as an effective solution to cope with this issue. In traditional WPT systems, specialized energy transmitters are installed at fixed locations to send Radiofrequency (RF) signals to charge IoT nodes, especially low-power ones. However, the range of these systems is limited by the low efficiency of end-to-end power transmission over long distances. Therefore, fixed-location energy

transmitters must be densely deployed to wirelessly recharge a large number of low-power devices, which would significantly increase the cost and hinder large scale implementation.

To tackle this issue, the majority of the scientific literature focuses on the combination of WPT and UAVs as a solution to support an IoT network in terms of power delivery and information transmission. In particular, they focus on the optimization of different aspects, such as the movements of the UAV [18]–[25], power allocation [19], [21]–[23], [25], [26], energy harvesting time [20]–[23], [26], [27], and the beamforming vectors of the antenna [24], [25].

To the best of the authors' knowledge, however, the state of the art does not consider the potential of satellites, and their integration with drones and WPT, as a comprehensive solution for IoT networks in harsh conditions.

Starting from the discussion above, this work combines together the advantages of these technologies by investigating a UAV-powered IoT-satellite integrated network, where a drone wirelessly recharges a set of Ground Nodes (GNs), while a LEO CubeSat provides connectivity for data exchange. Specifically, the objective is to achieve a fair maximization in terms of harvested energy and transmitted data.

The main contributions of this work are as follows:

- An integrated NTN is designed to enable the uplink data transmission of GNs to a LEO CubeSat, within its visibility window. These IoT nodes are deployed in a specific area and are recharged by a UAV, equipped with an array antenna, that employs WPT. Accordingly, a mathematical model is developed to characterize the UAV-GN channel and CubeSat-GN communication link.
- Two Mixed-Integer Non-Linear Programming (MINLP) problems are formulated to fairly maximize (i) the harvested energy of the GNs by jointly optimizing the UAV kinematics and the array antenna beamforming vectors, and (ii) the total transmitted data by fine-tuning the transmission plan of the nodes communicating with a LEO CubeSat. Both problems are non-convex and hence intractable. Therefore, the first is divided into two sub-problems, which are alternatively solved by leveraging also the Successive Convex Approximation (SCA) technique, until convergence to a quasi-optimal solution is achieved. Following a similar strategy, also the second problem is solved by adopting the two aforementioned techniques.
- A lower-bound mathematical expression for the harvested energy is derived. The stochastic nature of the UAV-GN channel model represents a challenge, which is addressed by imposing a maximum out-of-service probability. This leads to a non-linear energy-harvesting model that can be employed also for system design and assessment.
- A simulation campaign is conducted to prove the effectiveness of the proposed solution. In particular, multiple scenarios are analyzed and discussed under different parameter configurations, which include transmission power, number of GNs, and array antenna size. The performance of the conceived algorithm is then compared with a baseline approach, where the drone follows a snake-like trajectory and periodically recharges the nearest node by adopting an optimal transmission scheduling. Numerical results demonstrate that the proposed strategy outperforms the baseline in terms of total transmitted data.

The rest of the work is organized as follows: Section III describes the adopted system model. Sections VI and VII discuss the conceived problems' formulations and the proposed solutions. Section VIII presents the obtained numerical results. Finally, Section IX concludes the work and draws future research perspectives.

Notations: boldface lower case letters refer to vectors; $j = \sqrt{-1}$ is the imaginary unit; $\mathbf{x}^{\mathsf{T}}$ is the transpose of a generic vector $\mathbf{x}$; $\mathbf{x}^{\mathsf{H}}$ is the Hermitian of a generic vector $\mathbf{x}$; $\mathbf{x} \otimes \mathbf{y}$ denotes the Kronecker product between two generic vectors; $x \sim \mathcal{CN}(\mu, \sigma^2)$ define a circularly symmetric complex Gaussian distribution x with mean μ and variance σ^2; $\mathbf{I}_x$ represents the identity matrix of dimension x; $J_x(\cdot)$ denotes Bessel function of the first kind of order x; $\mathcal{O}(x)$ denotes the time-complexity of an algorithm of input size x, i.e, big O notation. The most significant parameters used in this work are summarized in Table I.

II. RELATED WORK

The scientific literature is currently focusing on enhancing traditional IoT networks by (i) expanding their coverage and (ii) improving the battery life of the devices.

Regarding the former, some intriguing contributions include the design of (i) communication and protocol schemes by adapting terrestrial technology to the space segment [28], (ii) resource allocation schemes able to improve energy efficiency [29], and (iii) more reliable LEO satellite-terrestrial communication techniques [30].

In this context, UAVs employed as mobile base station represent a valuable methodology to achieve ubiquitous connectivity. For instance, the authors in [31] aim at improving the perceived network quality by the user and minimizing the communication outages, while enhancing the data rate and the fairness of the transmission. Most noteworthy scientific efforts placed a great emphasis on the pairing of these two technologies by defining a hybrid network that leverages UAVs as relays to support satellite communications. In this context, the spectral efficiency and the outage probability are optimized in [32] by proposing a UAV relay selection and power allocation scheme. Other contributions design the transmission scheduling and the UAV trajectory to increase the system capacity [33] and energy efficiency through Non-Orthogonal Multiple Access (NOMA) [34].

For what concerns the battery life of the devices, WPT emerged as a disruptive technology for energy harvesting [35]. For instance, the authors in [36] propose a method that allows a node to first gather energy and then use it to transmit. Specifically, they investigate the optimal duration of a timeslot in a Time Division Multiple Access (TDMA) protocol, which maximizes the spectrum efficiency. Other approaches also consider the presence of a Intelligent Reflecting Surface (IRS) [37] to maximize the transferred power [38] and the throughput [39] of the users.

Moreover, cutting-edge approaches integrated the potential of WPT technology with the high mobility of the UAVs. A first setup is envisioned in [40] and [41], where energy-constrained nodes are optimally served by a UAV which acts as a base station, powered by WPT.

Recent works are also exploring the employment of UAV as a standalone WPT source. Clearly, one of the most critical aspects to be optimized is the UAV trajectory, which affects many facets of the mission, such as (i) the total amount of collected data [23], (ii) the age of information [27], (iii) the energy harvested by the GNs [18], [19], [22], [24], [25], (iv) the out-of-service probability [20], and (v) the UAV power consumption [21]. In particular, a novel scheme aided by an IRS, which simultaneously addresses WPT and information transmission for IoT sensors, is proposed in [23]. The protocol is divided into two phases: in the first one the drone recharges the devices while in the second one gathers the data. The objective is to maximize the total network sum-rate by optimally deriving the trajectory, the power allocation, the energy harvesting scheduling of the nodes, and the phase-shift matrix of the surface. Furthermore, the authors in [27] investigate a scenario in which a UAV recharges the GNs, collects data, and then transfers them to a data center. The aim is to minimize the average age of information by jointly optimizing the UAV trajectory and the time allocated for WPT. Moreover, the approach proposed in [18] intervenes by supplying power at GNs with limited battery capacities deployed at remote areas. Given that UAV is employed as a wireless power supplier and data collector, its overall energy consumption must be optimized subject to task collection and resource budget requirements. In [20], it is discussed the minimization of the energy depletion of GNs, and hence their outage probability. The latter is subject to the UAV elevation angle and the time slot allocation between the energy harvesting and the information transmission of each GN. Finally, the authors in [21] study a scenario in which a UAV is in charge of sustaining the devices of a network by periodically flying back and forth from a fixed position. Two approaches are proposed to minimize the average UAV power consumption by determining the trajectory, the duration of working periods, and the charging phase. The works above, however, consider a single antenna to perform WPT. To fill the gap, the approaches proposed in [24] and [25] investigate the impact of an antenna array to increase energy efficiency by taking advantage of beamforming.

To the best of the authors' knowledge, there is a lack of contributions that design and evaluate the performance of a UAV-powered IoT network that relies on a LEO CubeSat for information transmission. In this regard, this work proposes an optimization strategy to fairly distribute energy via WPT operation across GNs, while maximizing the transmitted data.

III. SYSTEM MODEL

The entire mission, depicted in Figure 1, is divided into two phases. The first one considers a UAV wirelessly charging a set of G low-power GNs, while the second comprises the transmission of sensed data from the nodes to a LEO CubeSat.

The first phase is uniformly split into K timeslots of duration δ seconds each. The UAV flies at a fixed height z^U and
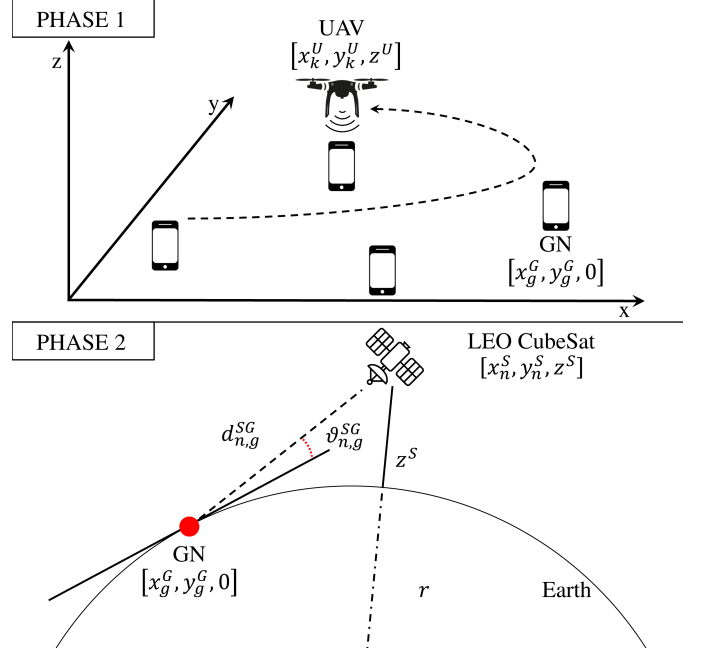

Fig. 1: Reference scenario.

follows a discretized trajectory, denoted by $\mathbf{q}_k^U = [x_k^U, y_k^U]^\mathsf{T} \in \mathbb{R}^2$, at a velocity of $\mathbf{v}_k^U \in \mathbb{R}^2$, with $k = 1, \ldots, K$. The GNs are uniformly deployed over an area of interest with a diameter equal to d^A and can be in either one of these three states: energy harvesting, data upload, and idle. Moreover, each one is placed at known coordinates denoted by $\mathbf{q}_g^G = [x_g^G, y_g^G]^\mathsf{T} \in \mathbb{R}^2$, with $g = 1, \ldots, G$. Therefore, it is possible to define the inclination and azimuth angles, i.e, $\theta_{k,g}^{UG}$ and $\varphi_{k,g}^{UG}$, between the g-th GN and the UAV as

$$\theta_{k,g}^{UG} = \arccos \frac{z^U}{d_{k,g}^{UG}}, \quad \varphi_{k,g}^{UG} = \arctan2 \frac{y_k^U - y_g^G}{x_k^U - x_g^G}, \quad (1)$$

and corresponding distance as:

$$d_{k,g}^{UG} = \sqrt{\|\mathbf{q}_k^U - \mathbf{q}_g^G\|^2 + (z^U)^2}. \quad (2)$$

Similarly to the former, also the second phase is split into N equal timeslots of duration δ seconds. The LEO CubeSat is assumed to be at constant altitude z^s, following a sun-synchronous circular orbit, denoted by $\mathbf{q}_n^s = [x_n^s, y_n^s]^\mathsf{T} \in \mathbb{R}^2$, with $n = 1, \ldots, N$, at steady speed $\mathbf{v}^s \in \mathbb{R}^2$.

Thus, the inclination $\theta_{n,g}^{SG}$ and azimuth $\varphi_{n,g}^{SG}$ angles, between the g-th GN and the LEO CubeSat read:

$$\theta_{n,g}^{SG} = \arccos \frac{z^s}{d_{n,g}^{SG}}, \quad \varphi_{n,g}^{SG} = \arctan2 \frac{y_n^s - y_g^G}{x_n^s - x_g^G}, \quad (3)$$

where the CubeSat-GN distance $d_{n,g}^{SG}$, also known as slant range [42], can be expressed as

$$d_{n,g}^{SG} = \sqrt{r^2 \sin^2 \vartheta_{n,g}^{SG} + (z^s)^2 + 2z^s r} - r \sin \vartheta_{n,g}^{SG}, \quad (4)$$

with r representing the Earth's radius and $\vartheta_{n,g}^{SG} = \frac{\pi}{2} - \theta_{n,g}^{SG}$ being the elevation angle. Note that, $0 \leq \vartheta_{n,g}^{SG} \leq \pi/2$ and specifically $\vartheta_{n,g}^{SG} = 0$ at the sunrise and the sunset, while $\vartheta_{n,g}^{SG} = \pi/2$ when the CubeSat is over the GNs. Since the

Symbol	Description	Symbol	Description
N	Number of discrete timeslots for the transmission phase.	$\chi_{n,g}^{\text{SG}}$	Link budget for the link between the CubeSat and the GN.
K	Number of discrete timeslots for the charging phase.	$\Upsilon_{n,g}^{\text{SG}}$	Link noise power for the link between the CubeSat and the GN.
G	Number of GN.	$\Gamma_{n,g}^{\text{SG}}$	SNR of the link between the CubeSat and the GN.
δ	Duration of each timeslot, in seconds.	R_n^{SG}	Maximum achievable data rate of the CubeSat-GN link.
$\mathbf{q}_k^{\text{U}}$	Position of the UAV in cartesian coordinates.	B	GN-CubeSat channel bandwidth.
$\mathbf{v}_k^{\text{U}}$	Velocity of the UAV in meters per second.	MCL	Maximum Coupling Loss.
$\mathbf{q}_n^{\text{S}}$	Position of the CubeSat in cartesian coordinates.	$\Delta_{n,g}^{\text{SG}}$	Uplink coupling loss between the CubeSat and the g-th GN.
$d_{k,g}^{\text{UG}}$	Distance between the UAV and the g-th GN.	$\mathbf{v}^{\text{S}}$	Orbital speed of the CubeSat over Earth.
$d_{n,g}^{\text{SG}}$	Distance between the CubeSat and the g-th GN.	G^{E}	Earth's gravitational constant.
$\theta_{n,g}^{\text{SG}}$	Inclination angle between the CubeSat and the g-th GN.	M^{E}	Mass of the Earth, expressed in kilograms.
$\varphi_{n,g}^{\text{SG}}$	Azimuth angle between the CubeSat and the g-th GN.	v^{F}	CubeSat speed footprint over Earth in meters per second.
$\vartheta_{n,g}^{\text{SG}}$	Elevation angle between the CubeSat and the g-th GN.	F^{S}	CubeSat footprint diameter, expressed in meters.
r	Earth radius, expressed in meters.	T^{V}	CubeSat visibility time, expressed in seconds.
$\mathbf{\Lambda}$	Transmission scheduling plan.	$\theta_{k,g}^{\text{UG}}$	Inclination angle between the UAV and the g-th GN.
$\mathbf{\Omega}$	Recharge scheduling plan.	$\varphi_{k,g}^{\text{UG}}$	Azimuth angle between the UAV and the g-th GN.
$L_{n,g}^I$	Communication loss between the CubeSat and the g-th GN.	$\mathbf{h}_{k,g}$	Channel vector of the UAV-GN WPT link with Rician fading.
$G_{n,g}^{\text{S}}, G_{n,g}^{\text{G}}$	Antenna gain of LEO CubeSat and GN.	κ	Rician K-factor.
ζ	Free space phase constant.	$\gamma_{k,g}$	Channel gain of the UAV-GN WPT link.
ϱ	Effective radius of the CubeSat antenna.	$E_{k,g}$	Energy harvested by the g-th GN, expressed in Joules.
$f^{\text{SG}}, f^{\text{UG}}$	Carrier frequencies in Hertz.	$P, \bar{P}$	Transmission power of the UAV and the GNs in Watts.

TABLE I: Main notations used in this work.

altitude of the CubeSat is fixed, $d_{n,g}^{\text{SG}}$ depends only on the elevation angle. Finally, according to the scheduling plan $\mathbf{\Lambda} = (\lambda_{n,g}) \in \{0,1\}^{N \times G}$, if the energy harvested in the first phase is sufficient, then a GN can transmit the sensed data in the second one.

IV. DRONE MODEL

The UAV is equipped with an Uniform Planar Array (UPA), with $S = L \times W$ antenna elements, which works in one of the resonant frequencies of the GNs' monopole antenna. Beamforming is adopted in order to maximize the power transfer to the GN of interest. Typically, the air-to-ground links are characterized by a strong Line-of-Sight (LoS) component. However, the multi-path fading caused by reflections on the ground is not negligible. Therefore, the Rician distribution is adopted to capture both LoS and Non-Line-of-Sight (NLoS) components [43], thus granting a realistic representation of the UAV-GN channel. Consequently, following Rician fading, the channel vector for the Multiple-Input-Single-Output (MISO) link between the UAV and the g-th GN, characterized by the Rician K-factor κ, can be modeled as:

$$\mathbf{h}_{k,g} = \sqrt{\frac{\kappa}{\kappa+1}}\bar{\mathbf{h}}_{k,g} + \sqrt{\frac{1}{\kappa+1}}\tilde{\mathbf{h}}_{k,g} \in \mathbb{C}^{S \times 1}, \quad (5)$$

where

$$\bar{\mathbf{h}}_{k,g} = \left[1, e^{-j\ell d \sin\theta_{k,g}^{\text{UG}}\cos\varphi_{k,g}^{\text{UG}}}, \dots, e^{-j(W-1)\ell d \sin\theta_{k,g}^{\text{UG}}\cos\varphi_{k,g}^{\text{UG}}}\right]^{\mathsf{T}}$$
$$\otimes \left[1, e^{-j\ell d \sin\theta_{k,g}^{\text{UG}}\sin\varphi_{k,g}^{\text{UG}}}, \dots, e^{-j(L-1)\ell d \sin\theta_{k,g}^{\text{UG}}\sin\varphi_{k,g}^{\text{UG}}}\right]^{\mathsf{T}},$$

is the LoS deterministic component, which describes the large-scale fading phenomena, and $\tilde{\mathbf{h}}_{k,g} \sim \mathcal{CN}(\mathbf{0}, \mathbf{I}_S)$ is the NLoS stochastic fluctuation due to multi-path propagation. Moreover, d is the distance between each element of the UAV's UPA, $\ell = \frac{2\pi}{c}f^{\text{UG}}$, c is the speed of light, and f^{UG} the carrier frequency. Given the channel model description, the gain between the UAV and each GN can be expressed as:

$$\gamma_{k,g} = \left|\sqrt{\beta\left(d_{k,g}^{\text{UG}}\right)^{-2}}\mathbf{w}_k^{\mathsf{H}}\mathbf{h}_{k,g}\right|^2, \quad (6)$$

where β denotes the channel power gain at the reference distance of 1 m, and $\mathbf{w}_k \in \mathbb{C}^{S \times 1}$ is the beam-forming vector.

The energy harvested by each g-th GN from the UAV can be non-linearly modeled [38], [41] as:

$$E_{k,g} = \frac{\alpha_0 P \delta \gamma_{k,g}}{\alpha_1 P \gamma_{k,g} + \alpha_1^2}, \quad (7)$$

where P is the transmission power of the UAV, and $\alpha_0 = 0.399$, $\alpha_1 = 0.826$ are positive constants determined in [38], [44]. Note that the adopted non-linear model is preferred with respect to a linear one, since it improves the overall accuracy and better estimates the time required to recharge each GN.

V. SATELLITE MODEL

This Section discusses the model adopted to describe the uplink communication between the GNs and the LEO Cube-Sat, to derive an expression of the link budget, which is then employed to obtain the reciprocal visibility time, and hence the mission duration. Among the possible channel models available in the scientific literature [45], the proposed one aligns with the specifications outlined in 3GPP TR 38.811 [6]. It is worth mentioning that, since the locations of GNs and the trajectory of the satellite are known, a compensation of the frequency shift introduced by the Doppler effect can be always performed, and hence it is not taken into account. Moreover, the considered uplink channel is typically characterized by a large elevation angle of the LEO CubeSat with respect to GNs [46], thus leading to a communication link dominated by a strong LoS component and hence a negligible slow fading. Besides, the satellite is distant several hundred kilometers from the nodes, and hence the channel is subject to a significant pathloss which makes the multi-path effect negligible [47].

To avoid interference among different nodes, the communication system has been designed in a TDMA fashion, such that at most one node per timeslot can communicate with the LEO CubeSat. This comes with the advantage, differently from Frequency Division Multiple Access (FDMA), that the GNs can effectively exploit all the available bandwidth. Each GN

employs a Commercial Off-the-Shelf (COTS) horizontally-oriented monopole antenna, assumed to be lossless, with linear polarization that operates at frequency f^{SG} in the S-band [48].

In particular, the antenna gain [48] can be expressed solely as function of the elevation angle $\vartheta_{n,g}^{\text{SG}}$:

$$G_{n,g}^{\text{G}} = 4\,\frac{\cos^2\!\left(\frac{\pi}{2}\cos\vartheta_{n,g}^{\text{SG}}\right)}{\sin^2\vartheta_{n,g}^{\text{SG}}\int_0^\pi \frac{\cos^2\left(\frac{\pi}{2}\cos\vartheta\right)}{\sin\vartheta}d\vartheta}. \tag{8}$$

Likewise, the LEO CubeSat is equipped with a lossless circular patch antenna, whose gain [48] can be expressed as:

$$G_{n,g}^{\text{s}} = 4\,\frac{\cos^2\varphi_{n,g}^{\text{SG}}J_{02}'^2 + \cos^2\theta_{n,g}^{\text{SG}}\sin^2\varphi_{n,g}^{\text{SG}}J_{02}^2}{\int_0^{\pi/2}(J_{02}'^2 + \cos^2\theta J_{02}^2)\sin\theta d\theta}. \tag{9}$$

Specifically, J_{02}' and J_{02} read:

$$J_{02}' = J_0(\zeta\varrho\sin\theta_{n,g}^{\text{SG}}) - J_2(\zeta\varrho\sin\theta_{n,g}^{\text{SG}}), \tag{10}$$

$$J_{02} = J_0(\zeta\varrho\sin\theta_{n,g}^{\text{SG}}) + J_2(\zeta\varrho\sin\theta_{n,g}^{\text{SG}}), \tag{11}$$

with ζ being the free space phase constant and ϱ the effective radius. Furthermore, the channel is characterized by different impairments [49] which can be modeled as follows:

$$L_{n,g}^{\text{I}} = L_{n,g}^{\text{A}}\,L_{n,g}^{\text{R}}\,L_{n,g}^{\text{Sc}}\,L^{\text{P}}. \tag{12}$$

In particular, $L_{n,g}^{\text{I}}$ is estimated by taking into account the air attenuation and the atmospheric gas absorption $L_{n,g}^{\text{A}}$ [50]–[52], the rainfall droplet $L_{n,g}^{\text{R}}$ [53], [54], the scintillation attenuation $L_{n,g}^{\text{Sc}}$ [48], and the polarization attenuation L^{P} [48]. The transmitted signal of each GN undergoes polarization rotation during the propagation in the ionosphere. It means that the signal may be polarized differently than intended on the satellite side. This phenomenon can be mitigated by using a circular-polarized signal, causing a maximum misalignment of $\pi/4$, which leads to $L^{\text{P}} = 2$. Therefore, the combination of (8), (9), and (12) leads to the definition of the link budget [49]:

$$\chi_{n,g}^{\text{SG}} = \frac{\overline{P}\,G_{n,g}^{\text{s}}\,G_{n,g}^{\text{G}}}{L_{n,g}^{\text{FS}}\,L_{n,g}^{\text{I}}}, \tag{13}$$

where $\overline{P}$ defines the transmission signal power of the GN.

Further, $L_{n,g}^{\text{FS}}$ [6] describes the free space propagation loss, which depends on the carrier frequency* f^{SG} and the GN-CubeSat distance $d_{n,g}^{\text{SG}}$.

Moreover, the receiver sensitivity [49] represents the noise power of the link and is defined as

$$\Upsilon_{n,g}^{\text{SG}} = k_B\,\eta_{n,g}^{\text{SG}}\,B, \tag{14}$$

with k_B being the Boltzmann constant, B the channel bandwidth, and η^{SG} describing the equivalent system noise temperature for both antenna and receiver noise.

Once the link budget and the receiver sensitivity are defined, it is possible to obtain the Signal-to-Noise Ratio (SNR) as:

$$\Gamma_{n,g}^{\text{SG}} = \frac{\chi_{n,g}^{\text{SG}}}{\Upsilon_{n,g}^{\text{SG}}}. \tag{15}$$

---

*It is assumed that f^{UG} and f^{SG} are different carriers defined in the S-band, such that the GN can employ the same monopole antenna for both information transmission and energy harvesting without interference.
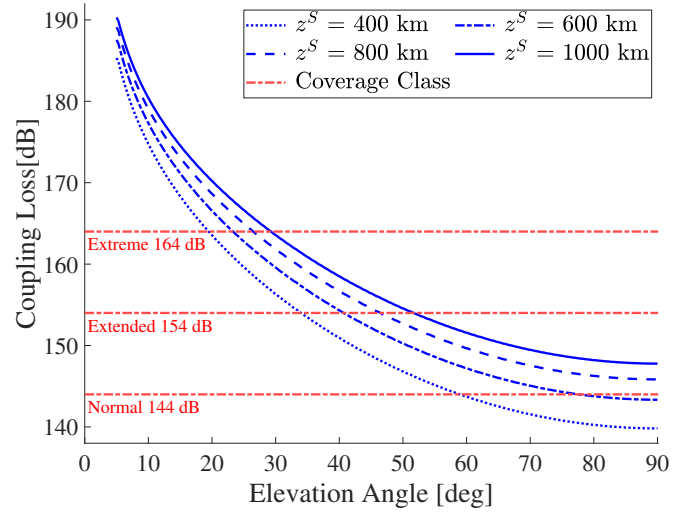

Fig. 2: Maximum Coupling Loss thresholds of the coverage classes for different CubeSat's altitudes [56].

To evaluate the coverage of a radio access technology, the 3GPP introduced the Maximum Coupling Loss (MCL) [55], which expresses the maximum loss in conducted power level, that a system may tolerate to properly establish a connection:

$$MCL = \frac{\overline{P}}{\hat{P}}, \tag{16}$$

where $\hat{P}$ is the minimum power required by the CubeSat to correctly decode the received signal. Therefore, it is possible to express the current uplink coupling loss for the g-th GN in the n-th timeslot as:

$$\Delta_{n,g}^{\text{SG}} = \frac{\overline{P}}{\chi_{n,g}^{\text{SG}}}. \tag{17}$$

Specifically, the GN is able to communicate with the CubeSat if and only if

$$\Delta_{n,g}^{\text{SG}} \leq MCL. \tag{18}$$

It is worth noting that $\Delta_{n,g}^{\text{SG}}$ is inversely proportional to $d_{n,g}^{\text{SG}}$, and hence to the elevation angle $\vartheta_{n,g}^{\text{SG}}$. The minimum elevation angle able to satisfy (18) is denoted as $\vartheta_{\text{MIN}}^{\text{SG}}$ and the period during $\vartheta_{\text{MIN}}^{\text{SG}} \leq \vartheta_{n,g}^{\text{SG}}$ is called reciprocal visibility time. Although the function of the coupling loss is dependent on non-invertible components [50]–[54], $\vartheta_{\text{MIN}}^{\text{SG}}$ can be obtained by intersecting the coupling loss curve with the MCL thresholds defined by the standard, also called coverage classes, shown in Figure 2.

Proposition 1. *Without loss of generality, if the diameter of the area of interest is much smaller than the footprint of the CubeSat, its distance from each GN, defined in (4), is approximately the same and can be expressed as d_n^{SG}.*

As a consequence of Proposition 1, it is considered the same reciprocal visibility period for each GN, which in turn defines the total duration of the second phase δN, as derived hereby.

The orbital period T^{s} of the CubeSat is denoted by the following equation:

$$T^{\text{s}} = 2\pi \sqrt{\frac{(r + z^{\text{s}})^3}{G^{\text{E}} M^{\text{E}}}}, \tag{19}$$

where M^{E} and G^{E} denote the mass and the gravitational constant of the Earth, respectively. Furthermore, the orbital speed v^{s} of an Earth's satellite is:

$$v^{\text{s}} = \sqrt{\frac{G^{\text{E}} M^{\text{E}}}{(r + z^{\text{s}})}} = \frac{2\pi(r + z^{\text{s}})}{T^{\text{s}}}. \tag{20}$$

Once defined the orbital speed v^{s}, it is necessary to compute the speed v^{F} of the covered area at the Earth side, namely footprint, as follows:

$$v^{\text{F}} = v^{\text{s}} - 2\pi \frac{z^{\text{s}}}{T^{\text{s}}} = 2\pi \frac{r}{T^{\text{s}}}. \tag{21}$$

Moreover, the footprint diameter F^S can be expressed by:

$$F^{\text{s}} = 2 z^{\text{s}} \tan(\theta_{\text{MIN}}^{\text{SG}}). \tag{22}$$

with $\theta_{\text{MIN}}^{\text{SG}} = \frac{\pi}{2} - \vartheta_{\text{MIN}}^{\text{SG}}$. Therefore, the duration δN, which corresponds to the visibility time T^{v} can be obtained as:

$$T^{\text{v}} \triangleq \delta N = \frac{F^{\text{s}}}{v^{\text{F}}} = \frac{2 z^{\text{s}} \tan(\theta_{\text{MIN}}^{\text{SG}})}{r} \sqrt{\frac{(r + z^{\text{s}})^3}{G^{\text{E}} M^{\text{E}}}}. \tag{23}$$

Finally, as a further consequence of Proposition 1, it is also possible to consider the same channel condition for each GN, and hence approximate Equation 15 as follows:

$$\Gamma_n^{\text{SG}} \simeq \Gamma_{n,g}^{\text{SG}} \forall g. \tag{24}$$

Hence, recalling the well-known Shannon formula [57], the maximum achievable data rate of a CubeSat-GN link is

$$R_n^{\text{SG}} = B \log_2(1 + \Gamma_n^{\text{SG}}). \tag{25}$$

VI. WIRELESS POWER TRANSFER OPTIMIZATION

Define $\mathbf{Q} = \{\mathbf{q}_k^{\text{U}}\}_{k=1}^K$, $\mathbf{V} = \{\mathbf{v}_k^{\text{U}}\}_{k=1}^K$, and $\mathbf{W} = \{\mathbf{w}_k\}_{k=1}^K$. The first phase concerning the kinematics of the drone and the node battery charging can be optimized by solving the following problem:

$$\max_{\eta_1, \mathbf{W}, \mathbf{Q}, \mathbf{V}} \eta_1 \quad \textbf{s.t.} \tag{26a}$$

$$\eta_1 \leq \sum_{k=1}^{K} E_{k,g}, \quad \forall g : 1, \ldots, G, \tag{26b}$$

$$\mathbf{q}_{k+1}^{\text{U}} = \mathbf{q}_k^{\text{U}} + \delta \mathbf{v}_k^{\text{U}}, \quad \forall k : 1, \ldots, (K-1), \tag{26c}$$

$$\mathbf{q}_1^{\text{U}} = \mathbf{q}_K^{\text{U}} = \mathbf{q}_0^{\text{U}}, \tag{26d}$$

$$\mathbf{v}_1 = \mathbf{v}_K = \mathbf{0}, \tag{26e}$$

$$\|\mathbf{v}_k\| \leq v_{\text{MAX}}, \quad \forall k : 1, \ldots, K, \tag{26f}$$

$$\|\mathbf{v}_{k+1} - \mathbf{v}_k\| \leq a_{\text{MAX}} \delta, \quad \forall k : 1, \ldots, (K-1). \tag{26g}$$

Problem (26) aims at fairly maximizing the battery charge of all the nodes through constraint (26b). Equation (26c) describes the kinematics of the drone, with the given initial and final point of the trajectory $\mathbf{q}_0^{\text{U}}$ and the correspondent speed imposed by (26d) and (26e), respectively. Moreover, (26f) and

(26g) limit the maximum speed and acceleration of the flight by v_{MAX} and a_{MAX}, respectively. However, (26) is a MINLP problem, and hence intractable in the present form. In particular, the stochastic formulation of the channel gain requires a dedicated strategy to derive an optimal solution. Therefore, the original problem is divided in two sub-problems, which are then alternately solved until convergence to a quasi-optimal solution is achieved.

A. Sub-Problem 1: Charge Plan Optimization

The first sub-problem aims at optimizing the beamforming vectors $\mathbf{W}$, such that the amount of energy harvested by the GNs is maximized in a fairly manner, as follows:

$$\max_{\eta_1, \mathbf{W}} \eta_1 \quad \textbf{s.t.} \quad (26b). \tag{27}$$

Still, (27) is non-convex in $\mathbf{W}$ due to constraint (26b), which is affected by the stochastic nature of the energy term $E_{k,g}$. To tackle this issue, the Maximum Ratio Combining [57] approach is adopted as beamforming strategy, which is indeed the optimal solution to maximize the energy harvested by a single GN:

$$\mathbf{w}_k = \frac{\mathbf{h}_{k,g}}{\|\mathbf{h}_{k,g}\|}. \tag{28}$$

Therefore, it is necessary to define a charging plan $\boldsymbol{\Omega} = (\omega_{k,g}) \in \{0, 1\}^{K \times G}$ describing which node is charged in each timeslot[†]. Hence, when a GN is selected, i.e., $\omega_{k,g} = 1$, the energy term $E_{k,g}$ can be rearranged combining (7) and (28) as

$$\widetilde{E}_{k,g} = \frac{\alpha_0 P \delta \beta \|\mathbf{h}_{k,g}\|^2}{\alpha_1 P \beta \|\mathbf{h}_{k,g}\|^2 + \alpha_1^2 \left(d_{k,g}^{\text{UG}}\right)^2}, \tag{29}$$

which, however, maintains a stochastic nature. Given an Out-of-Service probability ε, the minimum guaranteed energy $\overline{E}_{k,g}$ harvested by a GN, i.e, $\omega_{k,g} = 1$, can be obtained as follows:

$$\mathbb{P}\left(\widetilde{E}_{k,g} < \overline{E}_{k,g}\right) = \mathbb{P}\left(\|\mathbf{h}_{k,g}\|^2 < \frac{\alpha_1^2 \left(d_{k,g}^{\text{UG}}\right)^2 \overline{E}_{k,g}}{P\beta \left(\alpha_0 \delta - \alpha_1 \overline{E}_{k,g}\right)}\right)$$

$$= F\left(\frac{\alpha_1^2 \left(d_{k,g}^{\text{UG}}\right)^2 \overline{E}_{k,g}}{P\beta \left(\alpha_0 \delta - \alpha_1 \overline{E}_{k,g}\right)}\right) \leq \varepsilon, \tag{30}$$

with $F(\cdot)$ describing the Cumulative Distribution Function (CDF) of the stochastic energy expression $\widetilde{E}_{k,g}$ in (29). It is worth noting that the latter follows a non-central chi-squared distribution, and the correspondent CDF is

$$F(u) = 1 - Q_S\left(\sqrt{2S\kappa}, \sqrt{2(\kappa + 1)u}\right), \tag{31}$$

where $Q_S(\cdot)$ is the Marcum Q-function of order S.

[†]In this work, the side lobes that can eventually point to/illuminate other GNs are not considered, since their contribution is negligible.

Considering the worst-case scenario, in which (30) holds with equality, the final energy term $\overline{E}_{k,g}$ can be derived as

$$\overline{E}_{k,g} = \frac{\alpha_0 P \delta \beta \overline{Q}_S^2}{\alpha_1 P \beta \overline{Q}_S^2 + 2\alpha_1^2 \left(d_{k,g}^{\text{UG}}\right)^2 (\kappa+1)}, \tag{32}$$

$$\overline{Q}_S \triangleq Q_S^{-1}\left(\sqrt{2S\kappa}, 1-\varepsilon\right), \tag{33}$$

where $Q_S^{-1}(\cdot)$ is the inverse Marcum Q-function, which can be computed numerically or via analytical approximation. Figure 3 shows the CDF of $\widetilde{E}_{k,g}$ (left) defined in (31) and the derived energy term of $\overline{E}_{k,g}$ (right) obtained in (32). Therefore, problem (27) can be rearranged as

$$\max_{\eta_1, \mathbf{\Omega}} \eta_1 \quad \textbf{s.t.} \tag{34a}$$

$$\mathbf{\Omega} \in \{0,1\}^{K \times G}, \tag{34b}$$

$$\eta_1 \leq \sum_{k=1}^{K} \omega_{k,g} \overline{E}_{k,g}, \quad \forall g : 1, \ldots, G, \tag{34c}$$

$$\sum_{g=1}^{G} \omega_{k,g} \leq 1, \quad \forall k : 1, \ldots, K, \tag{34d}$$

where $E_{k,g}$ in (26b) has been substituted with (32). Moreover, constraints (34b) and (34d) impose that the drone can only recharge one sensor per timeslot. Still, (34) is non-convex due to the presence of the binary charging plan $\mathbf{\Omega}$. To cope with this issue, several works in the scientific literature employ only the relaxation of the integer constraint followed by a rounding procedure of the obtained values, which often results to be infeasible or far from optimal in the best case. To avoid such a scenario and to derive a quasi-integer solution, it is jointly employed (i) the relaxation of (34b), and (ii) an additional term in the objective function which encourages the adoption of a binary solution:

$$\max_{\eta_1, \mathbf{\Omega}} \eta_1 + \rho_1 \sum_{k=1}^{K} \sum_{g=1}^{G} \left(\omega_{k,g} - \frac{1}{2}\right)^2 \quad \textbf{s.t.} \tag{35a}$$

$$0 \leq \omega_{k,g} \leq 1, \quad \forall k : 1, \ldots, (K-1), \forall g : 1, \ldots, G, \tag{35b}$$

$$(34c), (34d).$$

In the above formulation, $\rho_1 \in \mathbb{R}^+$ acts as a weight that, if too low makes the additional term ineffective, otherwise if too high causes η_1 to become irrelevant. In the next Section, an empirical rule for the problem scaling, including ρ_1, will be discussed. Still, the objective function is non-convex with respect to $\mathbf{\Omega}$. To cope with this issue, the SCA technique is employed. Recalling that the first-order Taylor expansion is a global understimator for convex functions, it is possible to lower-bound the objective function for the local point $\overline{\omega}_{k,g}$, thus leading to the final formulation:

$$\max_{\eta_1, \mathbf{\Omega}} \eta_1 + \rho_1 \sum_{k=1}^{K} \sum_{g=1}^{G} \omega_{k,g}(2\overline{\omega}_{k,g} - 1) \quad \textbf{s.t.} \tag{36}$$

$$(34c), (34d), (35b).$$

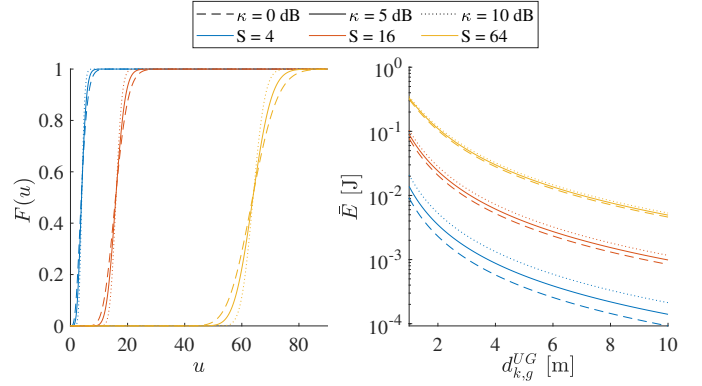It can be verified that (36) is convex.

Fig. 3: The CDF of the stochastic harvested energy $\widetilde{E}_{k,g}$ (left) and the minimum harvested energy $\overline{E}_{k,g}$ (right) with $\varepsilon = 0.01$ and $P = 49\,\text{dBm}$, for different number of antenna elements S and K-factor κ.

The scheduling plan is obtained by updating the value of the local point with the solution of the previous iteration, until convergence to a prescribed accuracy ξ is achieved.

Finally, since $\mathbf{\Omega} \in [0,1]^{K \times G}$, a round operation is performed. In particular, for each timeslot k, only the $\omega_{k,g}$ that has the maximum value is set to 1, while the others to 0. Therefore, constraints (34b) and (34d) are satisfied.

B. Sub-Problem 2: Drone Kinematics Optimization

Given the charging plan $\mathbf{\Omega}$ and the other results derived above, the trajectory-related parameters and the transmission plan are hereby optimized. Note that η_1 is re-optimized to derive a fair solution from the energy-harvesting perspective. The second sub-problem reads:

$$\max_{\eta_1, \mathbf{Q}, \mathbf{V}} \eta_1 \quad \textbf{s.t.} \tag{37}$$

$$(34c), (26c) - (26g),$$

which however is non-convex due to the presence of the squared distance term $d_{k,g}^{\text{UG}}$ at the denominator of $\overline{E}_{k,g}$ in constraints (34c). To tackle this issue, it is first necessary to introduce a set of slack variables $\mathbf{B} = \{b_{k,g} \geq 0\}$. Then, recalling the definition of the distance in (2), the slack variables are lower-bounded such that

$$\left(d_{k,g}^{\text{UG}}\right)^2 \leq b_{k,g}. \tag{38}$$

Similarly to the previous sub-problem, the SCA technique is employed which leads to the following inequality chain

$$\overline{\overline{E}}_{k,g} = \frac{\alpha_2}{\alpha_3 + \alpha_4 \overline{b}_{k,g}} - \frac{\alpha_2 \alpha_4}{\left(\alpha_3 + \alpha_4 \overline{b}_{k,g}\right)^2}(b_{k,g} - \overline{b}_{k,g}) \tag{39}$$

$$\overset{(a)}{\leq} \frac{\alpha_2}{\alpha_3 + \alpha_4 b_{k,g}} \overset{(b)}{\leq} \overline{E}_{k,g},$$

Algorithm 1: WPT Optimization.

Set $\mathbf{q}_g^{\mathrm{G}}$ and $\mathbf{q}_k^{\mathrm{S}}$;
Compute R_k^{SG} and $\overline{Q}_S$;
Initialize $\overline{b}_{k,g}, \overline{\omega}_{k,g}$;
for $m : 1, \ldots, M$ **do**
   for $i : 1, \ldots, I$ **do**
      Solve (36) to obtain the objective function $s_{1,i}, \eta_1$, and $\mathbf{\Omega}$;
      $\overline{\omega}_{k,g} \leftarrow \omega_{k,g} \; \forall k, g$;
      if $i > 1$ **and** $|s_{1,i} - s_{1,i-1}|/|s_{1,i}| < \xi$ **then**
         $s_{1,m}^* \leftarrow s_{1,i}$; **break**;
   end
   Round the optimized $\mathbf{\Omega}$;
   for $i : 1, \ldots, I$ **do**
      Solve (40) to obtain the objective function $s_{2,i}, \eta_1$, $\mathbf{Q}$, and $\mathbf{V}$;
      $\overline{b}_{k,g} \leftarrow b_{k,g} \; \forall k, g$;
      if $i > 1$ **and** $|s_{2,i} - s_{2,i-1}|/|s_{2,i}| < \xi$ **then**
         $s_{2,m}^* \leftarrow s_{2,i}$; **break**;
   end
   if $m > 1$ **and** $|s_{1,m}^* - s_{1,m-1}^*|/|s_{1,m}^*| < \xi$ **and** $|s_{2,m}^* - s_{2,m-1}^*|/|s_{2,m}^*| < \xi$ **then**
      break;
   Round and process the optimized $\mathbf{\Omega}$;
end

---

where (a) is due to the first order Taylor expansion, (b) follows from (38), $\alpha_2 \triangleq \alpha_0 P \delta \beta \overline{Q}_S^2$, $\alpha_3 \triangleq \alpha_1 P \beta \overline{Q}_S^2$, and $\alpha_4 \triangleq 2\alpha_1^2(\kappa + 1)$. Hence, problem (37) is equivalent to

$$\max_{\eta_1, \mathbf{Q}, \mathbf{V}, \mathbf{B}} \eta_1 \quad \textbf{s.t.} \tag{40a}$$

$$\eta_1 \leq \sum_{k=1}^{K} \omega_{k,g} \overline{\overline{E}}_{k,g}, \quad \forall g : 1, \ldots, G, \tag{40b}$$

$$(26\text{c}) - (26\text{g}),$$

because in order to maximize the objective function it is necessary to maximize the new energy term in (39) and hence minimize $b_{k,g}$, until (38) holds with equality. Therefore, problem (40) is convex with respect to $\mathbf{Q}, \mathbf{V}$, and $\mathbf{B}$ and it is iteratively solved until a prescribed accuracy ξ is achieved.

C. Overall Optimization Procedure

A quasi-optimal solution for the original problem (26) is derived by iteratively solving the two discussed sub-problems. It is worth specifying that, to avoid a waste of irradiated power, at the end of the entire procedure, the recharging plan $\mathbf{\Omega}$ is further improved by setting to zero the entries which do not satisfy a minimum harvested energy threshold ν, which typically takes place when the drone is too far from a specific node (as can be seen in Figure 3). For what concern the time complexity, the first sub-problem is in the order of $\mathcal{O}\left(I_1(KG+1)^{3.5}\right)$, where I_1 is the number of iterations required by SCA. Similarly, the second sub-problem has a complexity of $\mathcal{O}\left(I_2(4K + KG + 1)^{3.5}\right)$. Therefore, the joint complexity is given by $\mathcal{O}\left(M_1(I_1(KG+1)^{3.5} + I_2(4K + KG + 1)^{3.5})\right)$, where M_1 is denotes the number of iterations required to converge. More details can be found in Algorithm 1.

Algorithm 2: Transmission Optimization.

Set $\mathbf{q}_g^{\mathrm{G}}$ and $\mathbf{q}_k^{\mathrm{S}}$;
Compute R_k^{SG} and $\overline{Q}_S$;
Initialize $\overline{\lambda}_{k,g}$;
for $i : 1, \ldots, I$ **do**
   Solve (42) to obtain the objective function $s_{3,i}, \eta_2$, and $\mathbf{\Lambda}$;
   $\overline{\lambda}_{n,g} \leftarrow \lambda_{n,g} \; \forall n, g$;
   if $i > 1$ **and** $|s_{3,i} - s_{3,i-1}|/|s_{3,i}| < \xi$ **then**
      $s_3^* \leftarrow s_{3,i}$; **break**;
end
Rectify the optimized $\mathbf{\Lambda}$;

VII. GROUND NODES-SATELLITE TRANSMISSION OPTIMIZATION

Leveraging the results obtained in the previous optimized phase, i.e., the energy $E_{k,g}$ harvested by the GNs, the second phase encompassing the GNs' transmission scheduling can be optimized by deriving the optimal solution of the following problem:

$$\max_{\eta_2, \mathbf{\Lambda}} \eta_2 \quad \textbf{s.t.} \tag{41a}$$

$$\mathbf{\Lambda} \in \{0, 1\}^{K \times G}, \tag{41b}$$

$$\eta_2 \leq \sum_{n=1}^{N} \lambda_{n,g} R_n^{\mathrm{SG}}, \quad \forall g : 1, \ldots, G, \tag{41c}$$

$$\delta \overline{P} \sum_{n=1}^{N} \lambda_{n,g} \leq \sum_{k=1}^{K} E_{k,g}, \quad \forall g : 1, \ldots, G, \tag{41d}$$

$$\sum_{g=1}^{G} \lambda_{n,g} \leq 1, \quad \forall k : 1, \ldots, K. \tag{41e}$$

Problem (41) focuses on fairly maximizing the sum-rate of all CubeSat-GN links through constraint (41c). Moreover, (41d) states that a GN can transmit only if enough energy has been harvested. Constraints (41b) and (41e) impose that only a GN can transmit in each timeslot. However, also (41) is a MINLP problem and hence non-convex due to (41b), which describes the binary nature of the transmission plan $\mathbf{\Lambda}$. Following the same rationale adopted to convexify problem (34), the binary constraint (41b) is relaxed and a new constraint is added to the formulation. Again, to encourage the adoption of an integer solution, one more addendum is introduced in the objective function employing the SCA method, thus leading to:

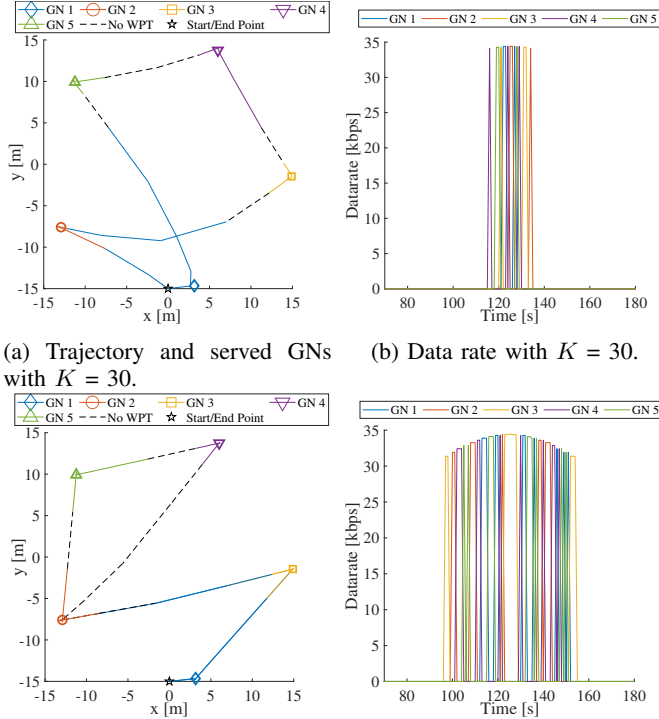$$\max_{\eta_2, \mathbf{\Lambda}} \eta_2 + \rho_2 \sum_{n=1}^{N} \sum_{g=1}^{G} \lambda_{n,g}(2\overline{\lambda}_{n,g} - 1) \quad \textbf{s.t.} \tag{42a}$$

$$0 \leq \lambda_{n,g} \leq 1, \quad \forall n : 1, \ldots, N, \forall g : 1, \ldots, G, \tag{42b}$$

$$(41\text{c}) - (41\text{e}).$$

The above formulation is convex and it is iteratively solved until a prescribed accuracy ξ is achieved. Similarly to (36), $\mathbf{\Lambda}$ needs to be rectified to satisfy (41b). However, in this case, $\lambda_{k,g}$ is rounded to 1 only if the value is ≥ 0.99, otherwise it is set to zero. This operation guarantees that the transmission takes place only if the scheduled GN has sufficient energy.

Parameter	Value	Parameter	Value
K	$\{30, 60\}$ [#]	N	250 [#]
G	$\{5, 10, 15\}$ [#]	B	180 [kHz]
L, W	$\{15, 20\}$ [#]	δ	1 [s]
$\mathbf{q}_0^{\text{U}}$	$[0, -15]$ [m]	$\mathbf{q}_0^{\text{S}}$	$[-795, 0]$ [km]
z^{U}	1 [m]	z^{S}	1000 [km]
v_{MAX}	15 [m/s]	$\mathbf{v}^{\text{S}}$	$[6353, 0]$ [m/s]
a_{MAX}	3 [m/s^2]	$\vartheta_{\text{MIN}}^{\text{SG}}$	52 [deg]
f^{UG}	2.4 [GHz]	f^{SG}	1995 [MHz]
ζ	0.42 [#]	ϱ	3.05 [cm]
η^{SG}	615 [K]	ν	0.005 [#]
ρ_1	0.01 [#]	ρ_2	2000 [#]
P	$\{46, 49\}$ [dBm]	$\overline{P}$	23 [dBm]
κ	10 [dB]	MCL	154 [dB]
ξ	10^{-3} [#]	ε	10^{-2} [#]

TABLE II: Parameter settings.

Fig. 5: Convergence of the algorithms with $G = 5$, $S = 225$, $P = 49$ dBm, and $\delta = 1$ s.

Fig. 6: Average harvested energy for different parameters with $\delta = 1$ s.
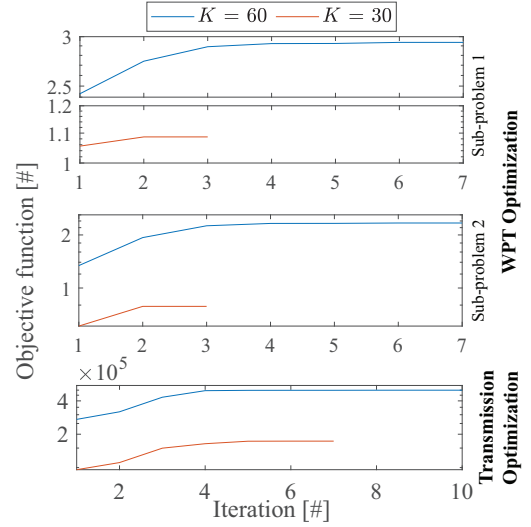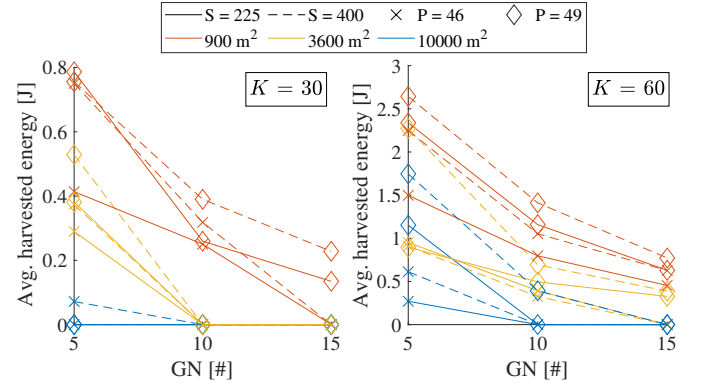

(a) Trajectory and served GNs with $K = 30$.

(b) Data rate with $K = 30$.

(c) Trajectory and served GNs with $K = 60$.

(d) Data rate with $K = 60$.

Fig. 4: Analysis of the scenario with $G = 5$, $S = 225$, $P = 49$ dBm, and $\delta = 1$ s.

The time complexity associated with the reference problem is in the order of $\mathcal{O}\left(I_3(KG + 1)^{3.5}\right)$, where I_3 is the number of iterations required by SCA. More details of the overall proposed algorithm can be found in Algorithm 2.

VIII. NUMERICAL RESULTS AND DISCUSSION

In this Section, a simulation campaign is carried out to assess the effectiveness of the proposed solution, which consists in sequentially executing Algorithm 1 and Algorithm 2.

The investigated scenarios involve different area sizes, i.e., 30x30 m^2, 60x60 m^2, and 100x100 m^2, in which $\{5, 10, 15\}$ GNs are uniformly deployed. The LEO CubeSat pursues a trajectory that follows a uniform linear motion, starting from position $\mathbf{q}_0^{\text{s}}$ at velocity $\mathbf{v}^{\text{s}}$. The parameters characterizing

the CubeSat-GN link are set according to [28]. Furthermore, considering a noise figure of 5 dB, the equivalent system noise temperature $\eta^{\text{SG}} \simeq 615$ K [48] is the sum of the antenna noise temperature and the receiver noise temperature, which correspond to 290 K and 150 K, respectively. Moreover, the UAV is equipped with a squared UPA of $\{255, 400\}$ elements to wirelessly recharge each GN at $\{46, 49\}$ dBm.

The transmission power is set in compliance with the ITU-R M.2135-1 Report [58], [59] for a Long Term Evolution (LTE) macro-cell deployed in urban and rural areas. All the simulation parameters are summarized in Table II.

A detailed discussion of the results, obtained by varying the aforementioned parameters, is followed by a comparison between the proposed solution and a baseline approach.

A. Objective function scaling

The normalization of the objective functions of both problems is deemed necessary, since their components have different orders of magnitude, which affect the optimization process, and hence the final solution. The possible values of η_1, given
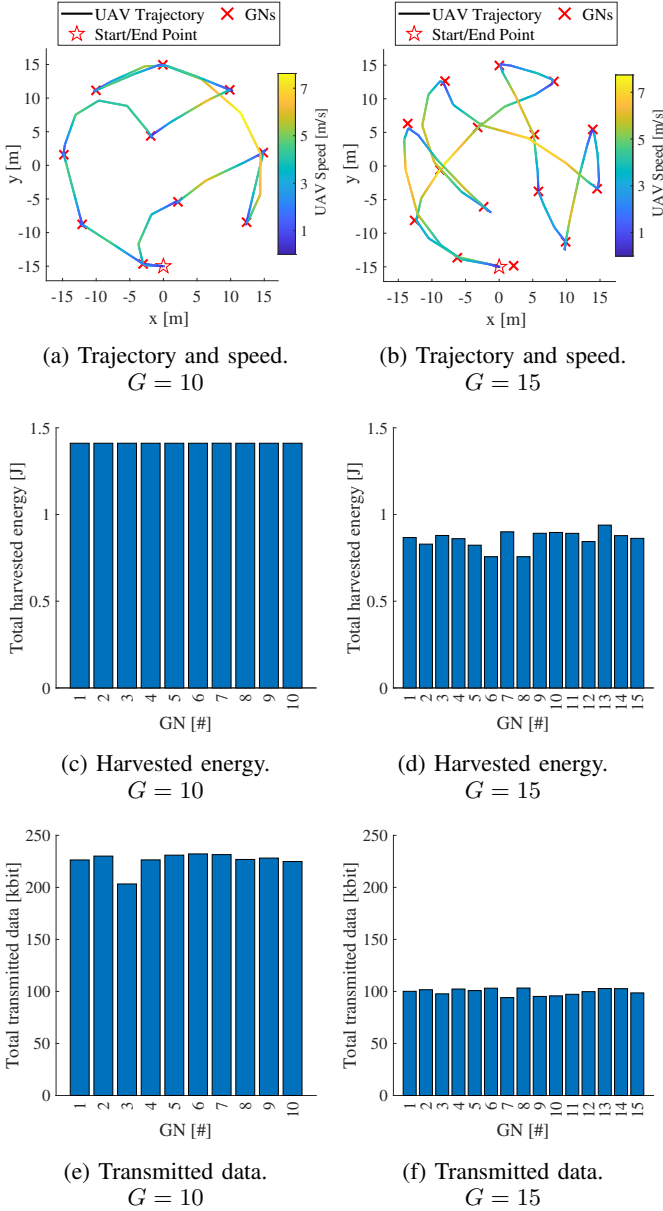
(a) Trajectory and speed.
$G = 10$

(b) Trajectory and speed.
$G = 15$

Fig. 8: Example of the UAV trajectory and speed in the baseline scenario with $G = 15$ with $K = 60$, $\delta = 1\,\mathrm{s}$.

(c) Harvested energy.
$G = 10$

(d) Harvested energy.
$G = 15$

(e) Transmitted data.
$G = 10$

(f) Transmitted data.
$G = 15$

Fig. 7: Analysis of the scenarios with $G = \{10, 15\}$, $S = 400$, $P = 49\,\mathrm{dBm}$, $K = 60$, $\delta = 1\,\mathrm{s}$.

the involved parameters of problem (26), range from $\sim 10^{-1}$ to ~ 1, as can be verified by solving the relaxed problem (36), with $\rho_1 = 0$. Accordingly, to keep the fairness factor slightly above the additional term introduced to encourage integer solutions, the following $\rho_1 = 10^{-2}$ is adopted. The same rationale is applied for problem (42), thus leading to $\rho_2 = 2 \cdot 10^3$.

B. Analysis of the results

The first scenario considers $G = 5$ GNs recharged by a drone equipped with a UPA of $S = 225$ elements, with $P = 49\,\mathrm{dBm}$ and $K = \{30, 60\}$. Indeed, the goal is to highlight how the duration of the first phase affects the second one in terms of obtained GNs' data rate. In this regard, Figures 4a and 4c jointly depict (i) the trajectory followed by the
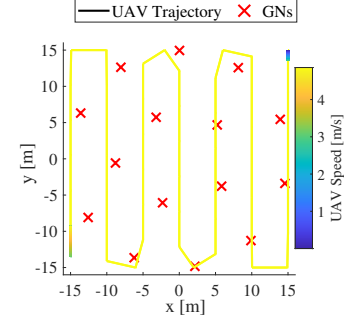
drone, and (ii) the GN recharged during the flight, and (iii) the initial position of the UAV, which is coincident with its final one. As it can be seen, in both scenarios, the trajectory paths tend to be straight to save time, which is convenient to reduce the distance between the UAV and the served GN, thus maximizing the energy income. It is worth noting that, thanks to the procedure performed at the end of the recharging phase, the drone does not irradiate power when is too far from the served GN, thus saving energy that would be not efficiently harvested by the nodes.

Furthermore, Figures 4b and 4d represent the data rate of nodes-satellite communications. It can be observed that the data rates are subject to the pathloss which affects the satellite link. Indeed, the satellite trajectory is designed to firstly approach and then leave the reference area, thus leading to increasing and then decreasing data rates, that visually resemble a parabola. In both configurations, the latter is centered around the mid-point of the mission to maximize the overall sum-rate. However, for higher K, the effective transmission time of the second phase increases and, as a consequence, the shape of the parabola changes. This phenomenon is due to the fact that more energy is harvested in the recharging phase. Therefore, the maximum data rate of $\sim 35\,\mathrm{kbps}$ is achieved always at $\sim 125\,\mathrm{s}$, which corresponds to the instant where the distance is minimized, i.e., the satellite is almost orthogonal to the area. Instead, the minimum data rates achieved are $\sim 34\,\mathrm{kbps}$ for $K = 30$ and $\sim 31\,\mathrm{kbps}$ for $K = 60$. Moreover, according to the constraints (41b) and (41e) which model the TDMA protocol, the peaks of the curves never overlap. For the sake of completeness, Figure 5 shows the convergence curves of the proposed optimization algorithms, specifically related to the first and second phases. It is noteworthy that in the two chosen configurations, Algorithm 1 achieves convergence after 7 iterations at most, while Algorithm 2 after 10 iterations, both with a prescribed accuracy of ξ.

To further investigate the impact on the harvested energy when the parameters involved in the scenario vary, Figure 6 shows the average amount collected by a GN. As expected, most of the unfeasible, i.e., no harvested energy, configurations involve a 100x100 m^2 area. Indeed, the speed and acceleration limits of the drone, together with the maximum duration of the second phase, play the most important role in the mission feasibility. Clearly, also the transmission power and the number
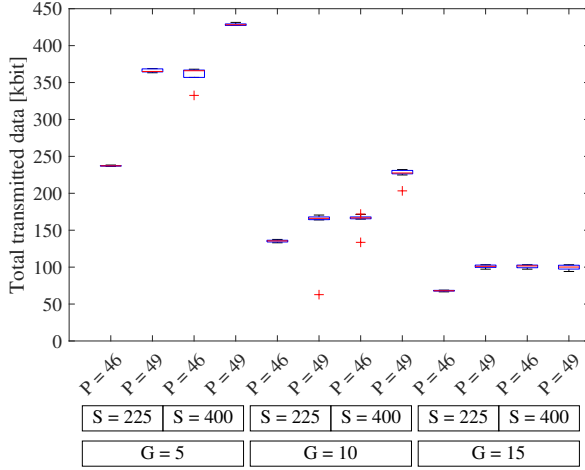
(a) Proposed algorithm.
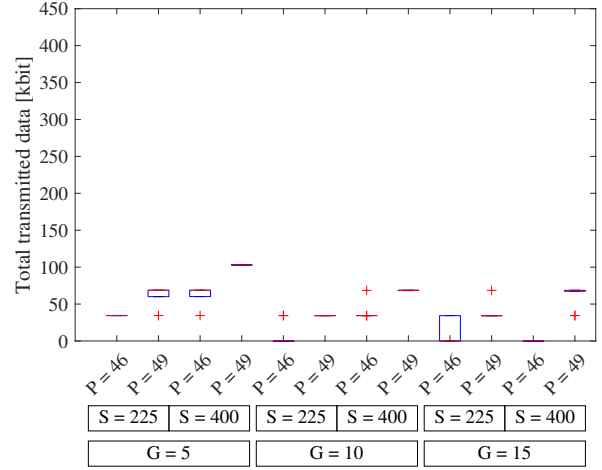
(b) Baseline algorithm.

Fig. 9: Comparison of the total transmitted data between the proposed solution and the baseline with $K = 60$, $\delta = 1\,\text{s}$.

of antenna elements are aspects that can also zero out the gathered energy, especially for a significant number of GNs. This result is of fundamental importance for the following analysis, since it provides a solid indication of which other configurations can be studied. It is worth mentioning that, across all the examined scenarios, the energy consumption of the UAV, which can be calculated with [60, Eq. 12], is significantly lower than the commonly used commercial drones.

To provide further insights, two more configurations are investigated with $G = \{10, 15\}$, $S = 400$, and $P = 49\,\text{dBm}$. Figures 7a and 7b illustrate the trajectory and the speed of the drone. Clearly, in both setups, the UAV slows down and approaches the GNs as close as possible to increase the amount of harvestable energy. Indeed, the speed of the drone reaches a maximum of $\sim 8\,\text{m/s}$.

This behaviour is reflected in Figures 7c and 7d, where the total harvested energy per GN in both configurations is depicted. As a matter of fact, the proposed approach presents satisfactory results in terms of fairness. Moreover, it can be observed that the average amount of harvested energy decreases from $\sim 1.4\,\text{J}$ with $G = 10$ to $\sim 0.9\,\text{J}$ with $G = 15$. This in turn leads to a different amount of transmitted data (Figures 7e and 7f) with a mean of $\sim 225\,\text{kbit}$ and $\sim 100\,\text{kbit}$, with a coefficient of variation of 0.037 and 0.031, respectively.

In conclusion, to prove its effectiveness, the proposed solution is compared to a baseline approach across all previously investigated scenarios. Specifically, the baseline foresees the drone covering the interest area by following a sampled snake-like trajectory at the minimum possible speed which satisfies the mission duration. The drone periodically recharges the battery of the nearest node throughout the flight. Subsequently, the final state of charge for each GN serves as input for Algorithm 2, which will endeavor to fairly distribute the available transmission resources. An instance of the UAV trajectory and its speed is shown in Figure 8.

The results of the comparison between the proposed solution and the baseline, with $K = 60$ and $\delta = 1\,\text{s}$, is illustrated

in Figure 9. Each bar reports the distribution of the total transmitted data per each GN, for all the possible combinations of transmission power P, number of antenna elements S and number of GNs G. As it can be seen, the proposed solution achieves great performance when the number of GNs is small enough, i.e., $G = 5$, allowing the UAV to hover over each one as much as possible. Indeed, more energy harvested by each GN corresponds to a greater amount of data transmitted. The same holds true when P and S increase. Finally, the baseline does not always provide sufficient energy to the GNs for the transmission. Instead, the proposed method demonstrates a higher total transmitted data volume compared to the baseline approach, ranging from a minimum of 1.5 to a maximum of 7 times higher, due to its fairly optimized energy distribution.

IX. CONCLUSIONS

In this work, a Satellite-IoT network powered by a UAV via WPT has been investigated. Starting from the system model, two MINLP problems have been formulated to fairly maximize the harvested energy of the GNs and the total transmitted data towards a LEO CubeSat. This requires a joint optimization approach that encompasses recharge and transmission scheduling plans while accounting for drone kinematics. To handle the non-convexity of both problems, the former has been decomposed into two sub-problems and then reformulated by also applying SCA technique. Meanwhile, the latter is tackled by employing the same two aforementioned techniques. A simulation campaign has been conducted in order to evaluate the algorithm performance over different (i) number of GNs, (ii) number of antenna elements of the UAV, (iii) WPT transmission power levels, (iv) area sizes, and (v) mission duration. Finally, the proposed solution is compared with a reference baseline approach, demonstrating a substantial performance improvement, ranging from 1.5 to 7 times, in terms of the total amount of transmitted data.

In the future, the research efforts will be focused on the following directions:

- Extend the algorithm to multiple drones for a thoroughly integrated NTN cooperative network.
- Investigate inductive and capacitive WPT models to improve the overall efficiency.
- Employ 3D antenna arrays for a more flexible beam-steering and -forming strategies.
- Expand the trajectory optimization and GN placement considering different heights to address different terrain conditions.
- Consider the presence of a IRS that can enhance the energy harvested by GNs.
- Investigate the adoption of other multiple access protocols, such as random access scheme, FDMA, and NOMA.

Finally, the proposal will lay the groundwork for the realization of a testbed that will be used for experimentation and measurements in the context of 6G technologies.

REFERENCES

[1] "IMT Vision–Framework and overall objectives of the future development of IMT for 2020 and beyond," *Recommendation ITU*, vol. 2083, no. 0, 2015.

[2] H. Tataria, M. Shafi, M. Dohler, and S. Sun, "Six Critical Challenges for 6G Wireless Systems: A Summary and Some Solutions," *IEEE Vehicular Technology Magazine*, vol. 17, no. 1, pp. 16–26, 2022.

[3] M. Giordani, M. Polese, M. Mezzavilla, S. Rangan, and M. Zorzi, "Toward 6G Networks: Use Cases and Technologies," *IEEE Communications Magazine*, vol. 58, no. 3, pp. 55–61, 2020.

[4] H. Cui, J. Zhang, Y. Geng, Z. Xiao, T. Sun, N. Zhang, J. Liu, Q. Wu, and X. Cao, "Space-air-ground integrated network (SAGIN) for 6G: Requirements, architecture and challenges," *China Communications*, vol. 19, no. 2, pp. 90–108, 2022.

[5] J. Liu, Y. Shi, Z. M. Fadlullah, and N. Kato, "Space-Air-Ground Integrated Network: A Survey," *IEEE Communications Surveys & Tutorials*, vol. 20, no. 4, pp. 2714–2741, 2018.

[6] 3GPP, "Study on New Radio (NR) to support non-terrestrial networks (NTNs)," 3GPP, Technical Report (TR) 38.811, 2020, Version 15.2.0, Release 15.

[7] ——, "Solutions for NR to support Non-Terrestrial Networks (NTN)," 3GPP, Technical Report (TR) 38.821, 2023, Release 16.

[8] ——, "Non-terrestrial networks (NTN) related RF and co-existence aspects," 3GPP, Technical Report (TR) 38.863, 2022, Release 17.

[9] ——, "Study on requirements and use cases for network verified UE location for Non-Terrestrial-Networks (NTN) in NR," 3GPP, Technical Report (TR) 38.882, 2022, Release 18.

[10] M. M. Azari, S. Solanki, S. Chatzinotas, O. Kodheli, H. Sallouha, A. Colpaert, J. F. Mendoza Montoya, S. Pollin, A. Haqiqatnejad, A. Mostaani, E. Lagunas, and B. Ottersten, "Evolution of Non-Terrestrial Networks From 5G to 6G: A Survey," *IEEE Communications Surveys & Tutorials*, vol. 24, no. 4, pp. 2633–2672, 2022.

[11] M. Giordani and M. Zorzi, "Non-Terrestrial Networks in the 6G Era: Challenges and Opportunities," *IEEE Network*, vol. 35, no. 2, pp. 244–251, 2021.

[12] O. Kodheli, E. Lagunas, N. Maturo, S. K. Sharma, B. Shankar, J. F. M. Montoya, J. C. M. Duncan, D. Spano, S. Chatzinotas, S. Kisseleff, J. Querol, L. Lei, T. X. Vu, and G. Goussetis, "Satellite Communications in the New Space Era: A Survey and Future Challenges," *IEEE Communications Surveys & Tutorials*, vol. 23, no. 1, pp. 70–109, 2021.

[13] Z. Xiao, J. Yang, T. Mao, C. Xu, R. Zhang, Z. Han, and X.-G. Xia, "LEO Satellite Access Network (LEO-SAN) towards 6G: Challenges and Approaches," *IEEE Wireless Communications*, pp. 1–8, 2022.

[14] M. Mozaffari, X. Lin, and S. Hayes, "Toward 6G with Connected Sky: UAVs and Beyond," *IEEE Communications Magazine*, vol. 59, no. 12, pp. 74–80, 2021.

[15] P. Boccadoro, D. Striccoli, and L. A. Grieco, "An Extensive Survey on the Internet of Drones," *Ad Hoc Netw.*, vol. 122, p. 102600, 2021.

[16] D. C. Nguyen, M. Ding, P. N. Pathirana, A. Seneviratne, J. Li, D. Niyato, O. Dobre, and H. V. Poor, "6g internet of things: A comprehensive survey," *IEEE Internet of Things Journal*, vol. 9, no. 1, pp. 359–383, 2022.

[17] X. Lu, P. Wang, D. Niyato, D. I. Kim, and Z. Han, "Wireless Charging Technologies: Fundamentals, Standards, and Network Applications," *IEEE Communications Surveys & Tutorials*, vol. 18, no. 2, pp. 1413–1452, 2016.

[18] S. Zhang, W. Liu, and N. Ansari, "Joint Wireless Charging and Data Collection for UAV-Enabled Internet of Things Network," *IEEE Internet of Things Journal*, vol. 9, no. 23, pp. 23 852–23 859, 2022.

[19] J. Mu and Z. Sun, "Trajectory Design for Multi-UAV-Aided Wireless Power Transfer toward Future Wireless Systems," *Sensors*, vol. 22, no. 18, p. 6859, 2022.

[20] Y. Liu, K. Xiong, Y. Lu, Q. Ni, P. Fan, and K. B. Letaief, "UAV-aided wireless power transfer and data collection in Rician fading," *IEEE Journal on Selected Areas in Communications*, vol. 39, no. 10, pp. 3097–3113, 2021.

[21] Y. Hu, X. Yuan, G. Zhang, and A. Schmeink, "Sustainable wireless sensor networks with UAV-enabled wireless power transfer," *IEEE Transactions on Vehicular Technology*, vol. 70, no. 8, pp. 8050–8064, 2021.

[22] X. Mo, Y. Huang, and J. Xu, "Radio-map-based robust positioning optimization for UAV-enabled wireless power transfer," *IEEE Wireless Communications Letters*, vol. 9, no. 2, pp. 179–183, 2019.

[23] K. K. Nguyen, A. Masaracchia, V. Sharma, H. V. Poor, and T. Q. Duong, "RIS-assisted UAV communications for IoT with wireless power transfer using deep reinforcement learning," *IEEE Journal of Selected Topics in Signal Processing*, 2022.

[24] X. Yuan, H. Jiang, Y. Hu, and A. Schmeink, "Joint Analog Beamforming and Trajectory Planning for Energy-Efficient UAV-Enabled Nonlinear Wireless Power Transfer," *IEEE Journal on Selected Areas in Communications*, vol. 40, no. 10, pp. 2914–2929, 2022.

[25] X. Yuan, Y. Hu, and A. Schmeink, "Joint design of UAV trajectory and directional antenna orientation in UAV-enabled wireless power transfer networks," *IEEE Journal on Selected Areas in Communications*, vol. 39, no. 10, pp. 3081–3096, 2021.

[26] Z. Liu, S. Zhao, Q. Wu, Y. Yang, and X. Guan, "Joint Trajectory Design and Resource Allocation for IRS-Assisted UAV Communications With Wireless Energy Harvesting," *IEEE Communications Letters*, vol. 26, no. 2, pp. 404–408, 2022.

[27] H. Hu, K. Xiong, G. Qu, Q. Ni, P. Fan, and K. B. Letaief, "AoI-Minimal Trajectory Planning and Data Collection in UAV-Assisted Wireless Powered IoT Networks," *IEEE Internet of Things Journal*, vol. 8, no. 2, pp. 1211–1223, 2021.

[28] G. Sciddurlo, A. Petrosino, M. Quadrini, C. Roseti, D. Striccoli, F. Zampognaro, M. Luglio, S. Perticaroli, A. Mosca, F. Lombardi, I. Micheli, A. Ornatelli, V. Schena, A. D. Mezza, A. Mattioni, D. Morbidelli, G. Boggia, and G. Piro, "Looking at NB-IoT Over LEO Satellite Systems: Design and Evaluation of a Service-Oriented Solution," *IEEE Internet of Things Journal*, vol. 9, no. 16, pp. 14 952–14 964, 2022.

[29] H. Chelle, M. Crosnier, R. Dhaou, and A.-L. Beylot, "Adaptive Load Control for IoT Based on Satellite Communications," in *2018 IEEE International Conference on Communications (ICC)*, 2018, pp. 1–7.

[30] Z. Gao, A. Liu, C. Han, and X. Liang, "Non-Orthogonal Multiple Access-Based Average Age of Information Minimization in LEO Satellite-Terrestrial Integrated Networks," *IEEE Transactions on Green Communications and Networking*, vol. 6, no. 3, pp. 1793–1805, 2022.

[31] C. Zhan, H. Hu, X. Sui, Z. Liu, J. Wang, and H. Wang, "Joint Resource Allocation and 3D Aerial Trajectory Design for Video Streaming in UAV Communication Systems," *IEEE Transactions on Circuits and Systems for Video Technology*, vol. 31, no. 8, pp. 3227–3241, 2021.

[32] S. Mirbolouk, M. Valizadeh, M. C. Amirani, and S. Ali, "Relay Selection and Power Allocation for Energy Efficiency Maximization in Hybrid Satellite-UAV Networks With CoMP-NOMA Transmission," *IEEE Transactions on Vehicular Technology*, vol. 71, no. 5, pp. 5087–5100, 2022.

[33] Y. Wang, Z. Li, Y. Chen, M. Liu, X. Lyu, X. Hou, and J. Wang, "Joint Resource Allocation and UAV Trajectory Optimization for Space–Air–Ground Internet of Remote Things Networks," *IEEE Systems Journal*, vol. 15, no. 4, pp. 4745–4755, 2021.

[34] N. Wang, F. Li, D. Chen, L. Liu, and Z. Bao, "NOMA-Based Energy-Efficiency Optimization for UAV Enabled Space-Air-Ground Integrated Relay Networks," *IEEE Transactions on Vehicular Technology*, vol. 71, no. 4, pp. 4129–4141, 2022.

[35] C. R. Valenta and G. D. Durgin, "Harvesting Wireless Power: Survey of Energy-Harvester Conversion Efficiency in Far-Field, Wireless Power Transfer Systems," *IEEE Microwave Magazine*, vol. 15, no. 4, pp. 108–120, 2014.

[36] T. Terauchi, K. Suto, and M. Wakaiki, "Harvest-Then-Transmit-Based TDMA Protocol with Statistical Channel State Information for Wireless

Powered Sensor Networks," in *2021 IEEE 93rd Vehicular Technology Conference (VTC2021-Spring)*, 2021, pp. 1–5.

[37] C. Pan, H. Ren, K. Wang, J. F. Kolb, M. Elkashlan, M. Chen, M. Di Renzo, Y. Hao, J. Wang, A. L. Swindlehurst, X. You, and L. Hanzo, "Reconfigurable Intelligent Surfaces for 6G Systems: Principles, Applications, and Research Directions," *IEEE Communications Magazine*, vol. 59, no. 6, pp. 14–20, 2021.

[38] Z. Chu, P. Xiao, D. Mi, W. Hao, Z. Lin, Q. Chen, and R. Tafazolli, "Wireless Powered Intelligent Radio Environment with Non-Linear Energy Harvesting," *IEEE Internet of Things Journal*, pp. 1–1, 2022.

[39] D. Zhang, Q. Wu, M. Cui, G. Zhang, and D. Niyato, "Throughput Maximization for IRS-Assisted Wireless Powered Hybrid NOMA and TDMA," *IEEE Wireless Communications Letters*, vol. 10, no. 9, pp. 1944–1948, 2021.

[40] M. Wu, L. Su, J. Chen, X. Duan, D. Wu, Y. Cheng, and Y. Jiang, "Development and Prospect of Wireless Power Transfer Technology Used to Power Unmanned Aerial Vehicle," *Electronics*, vol. 11, no. 15, p. 2297, 2022.

[41] Z. Wang, T. Lv, J. Zeng, and W. Ni, "Placement and Resource Allocation of Wireless-Powered Multiantenna UAV for Energy-Efficient Multiuser NOMA," *IEEE Transactions on Wireless Communications*, pp. 1–1, 2022.

[42] M.-G. Kim and H.-S. Jo, "Performance Analysis of NB-IoT Uplink in Low Earth Orbit Non-Terrestrial Networks," *Sensors*, vol. 22, no. 18, 2022. [Online]. Available: https://www.mdpi.com/1424-8220/22/18/7097

[43] M. M. Azari, F. Rosas, K.-C. Chen, and S. Pollin, "Ultra Reliable UAV Communication Using Altitude and Cooperation Diversity," *IEEE Trans. Commun.*, vol. 66, no. 1, pp. 330–344, 2017.

[44] Y. Chen, N. Zhao, and M.-S. Alouini, "Wireless Energy Harvesting Using Signals From Multiple Fading Channels," *IEEE Transactions on Communications*, vol. 65, no. 11, pp. 5027–5039, 2017.

[45] V. M. Baeza, E. Lagunas, H. Al-Hraishawi, and S. Chatzinotas, "An Overview of Channel Models for NGSO Satellites," in *2022 IEEE 96th Vehicular Technology Conference (VTC2022-Fall)*, 2022, pp. 1–6.

[46] N. Okati, T. Riihonen, D. Korpi, I. Angervuori, and R. Wichman, "Downlink coverage and rate analysis of low earth orbit satellite constellations using stochastic geometry," *IEEE Transactions on Communications*, vol. 68, no. 8, pp. 5120–5134, 2020.

[47] Q. Chen, Z. Wang, G. F. Pedersen, and M. Shen, "Joint satellite-transmitter and ground-receiver digital pre-distortion for active phased arrays in leo satellite communications," *Remote Sensing*, vol. 14, no. 17, 2022.

[48] C. A. Balanis, *Antenna Theory: Analysis and Design, 2nd Edition*. Wiley, 1996.

[49] L. J.Ippolito, *Satellite Communications Systems Engineering: Atmospheric Effects, Satellite Link Design and System Performance, 2nd Edition*. Wiley, 2017.

[50] ITU, "Attenuation by atmospheric gases and related effects," International Telecommunication Union (ITU), Recommendation, 2019, ITU-R P.676-12.

[51] ——, "Attenuation due to clouds and fog," International Telecommunication Union (ITU), Recommendation, 2019, ITU-R P.840-8.

[52] ——, "Propagation data and prediction methods required for the design of Earth-space telecommunication systems," International Telecommunication Union, Tech. Rep., 2015, recommendations Radiowave Propag. ITU-R 618-12.

[53] ——, "Propagation data and prediction methods required for the design of Earth-space telecommunication systems," International Telecommunication Union (ITU), Recommendation, 2017, ITU-R P.618-13.

[54] ——, "Characteristics of precipitation for propagation modelling," International Telecommunication Union (ITU), Recommendation, 2021, ITU-R P.837-7.

[55] 3GPP, "Study on provision of low-cost Machine-Type Communications (MTC) User Equipments (UEs) based on LTE," 3rd Generation Partnership Project (3GPP), Tech. Rep. TR 36.888, 06 2013, Release 12.

[56] ——, "Medium Access Control (MAC) protocol specification," Evolved Universal Terrestrial Radio Access (E-UTRA), Tech. Rep. TS 36.321, 1 2020, version 15.8.0 Release 15.

[57] J. R. Barry, E. A. Lee, and D. G. Messerschmitt, *Digital communication*. Springer Science & Business Media, 2003.

[58] "Guidelines for evaluation of radio interface technologies for IMT-Advanced – Report ITU-R M.2135-1," International Telecommunication Union (ITU), Tech. Rep., 2009.

[59] Q. Zhang, G. Wang, J. Chen, G. B. Giannakis, and Q. Liu, "Mobile Energy Transfer in Internet of Things," *IEEE Internet of Things Journal*, vol. 6, no. 5, pp. 9012–9019, 2019.

[60] Y. Zeng, J. Xu, and R. Zhang, "Energy Minimization for Wireless Communication With Rotary-Wing UAV," *IEEE Trans. Wireless Commun.*, vol. 18, no. 4, pp. 2329–2345, Apr. 2019.

Giovanni Iacovelli received the Ph.D. in electrical and information engineering from Politecnico di Bari, Bari, Italy, in December 2022. His research interests include Internet of Drones, Machine Learning, Optimization and Telecommunications. Currently, he is an Assistant Professor in Telecommunications at the Department of Electrical and Information Engineering, Politecnico di Bari.

Giovanni Grieco received the Dr. Eng. degree (with honors) in Telecommunications Engineering from Politecnico di Bari, Bari, Italy in October 2021. His research interests include Internet of Drones, Cybersecurity, and Future Networking Architectures. He is the principal maintainer of IoD_Sim. Since 2021, he has been a Ph.D. student at the Department of Electrical and Information Engineering at Politecnico di Bari.
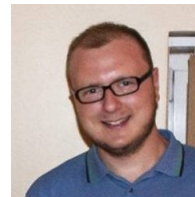
Antonio Petrosino obtained his Bachelor of Engineering in Computer Science and Automation, with a focus on Computer System and Software Engineering in 2016 and his Master degree (with honors) in Telecommunication Engineering in 2020. His research interests include Satellite Communication, Software-Defined Networking, Network Function Virtualization, and Internet of Things. Since 2020, he has been a Ph.D student at the Department of Electrical and Information Engineering at Politecnico di Bari.

L. Alfredo Grieco is a full professor in telecommunications at Politecnico di Bari. His research interests include Internet of Things, Future Internet Architectures, and Nano-communications. He serves as Founder Editor in Chief of the Internet Technology Letters journal (Wiley) and as Associate Editor of the IEEE Transactions on Vehicular Technology journal (for which he has been awarded as top editor in 2012, 2017, and 2020).

Gennaro Boggia received the Dr.Eng. and Ph.D. degrees (with Hons.) in electronics engineering from the Politecnico di Bari, Bari, Italy, in July 1997 and March 2001, respectively. He is a Full Professor of Telecommunication with the Politecnico di Bari, Bari, Italy. His research interests include wireless networking, cellular communication, protocol stacks for industrial applications and smart grids, Internet measurements, and network performance evaluation.